Journal of Directed Energy, **2**, Fall 2007, 285–296

Aero-Optical Measurements Using High-Bandwidth Two-Dimensional Wavefront Sensor Array

D. Cavalieri,* D. Wittich, and S. Gordeyev

Department of Aerospace and Mechanical Engineering, University of Notre Dame, Notre Dame, Indiana 46556

K. Cheung†

Oceanit, ASB Tower Suite 2970, 1001 Bishop Street, Honolulu, Hawaii 96813

and

E. Jumper

Department of Aerospace and Mechanical Engineering, University of Notre Dame, Notre Dame, Indiana 46556

High-speed compressible turbulent flows around an aircraft change the local index of refraction and impose optical aberrations on an airborne laser beam's wavefronts. These aberrations degrade the laser's beam ability to be focused in the far field, thus reducing its intensity on a target. It can be crucial for communication, interrogation, and targeting or as a directed energy weapon. Fast-evolving convecting turbulent structures that are present in turbulent flows usually exhibit high spatial and temporal bandwidths. Thus, measurement devices with high spatial and temporal resolutions are then required to accurately capture their evolution. Most commercially available two-dimensional wavefront sensors rely on a digital charge-coupled device camera and, although it usually provides an excellent spatial resolution, sampling rates are typically limited to a few hundred frames per second. These rates are far lower than desired sampling frequencies to correctly resolve optical aberrations, which are on the order of tens of thousands of hertz. We have developed a relatively inexpensive complementary analog device to accurately measure optical aberrations at high sampling rates. The device is an analog high-temporal-bandwidth, two-dimensional wavefront Shack–Hartmann sensor. It utilizes an 8 × 8 array of analog position sensing devices, and the sampling rates now are dramatically increased in excess of 78 kHz, with a respectable spatial resolution, i.e., 10-mm pitch. The high-bandwidth, two-dimensional wavefront sensor in this current configuration measures wavefronts over 64 subapertures. The device was tested on an acoustically forced, heated-jet facility and compared to a commercially available two-dimensional wavefront sensor with a 33 × 44 subaperture spatial resolution. We intend to show that the high-bandwidth sensor can correctly resolve all of the essential

Received March 23, 2006; revision received June 15, 2007.

*Corresponding author; e-mail: dcavalie@nd.edu.

†E-mail: kcheung@oceanit.com.

features of the roll-up structure evolution, including the convective nature and amplitude of the optical aberration and pairing of roll-up structures.

KEYWORDS: Aero-optics, OPD, Optical path difference, Wavefront measurements

Nomenclature

D	diameter
$\boldsymbol{d}$	displacements
f	focal distance
grad( )	gradient of expression ( )
WF	wavefront

1. Introduction

When a collimated laser beam travels through a medium with a variable index of refraction, its wavefront gets distorted. When the transmission distance through the medium is relatively small and the aberrations are caused by a flow with a changing density field, these effects are called aero-optical effects.[6] High-speed compressible turbulent flows around an aircraft change the local index of refraction and impose fast-changing optical aberrations on an airborne laser beam's wavefronts. These aberrations degrade the laser beam's ability to be focused in the far field, thus reducing its intensity on a target. The reduction in the intensity on target causes a reduction in system performance for communication, interrogation, and targeting or a directed energy weapon system.[14]

Until relatively recently the full impact of aero-optical effects on airborne direct energy laser weapon systems was not understood. Only in recent years have actual optical measurements of the aberrating environment imposed by separated flows over the exit pupils of the beam directors been shown to greatly limit the lethal field of regard of the weapons systems. Measurements made at the Arnold Engineering and Development Center and at the University of Notre Dame for flight Mach number conditions from 0.7 to 0.8 showed that the aberrating environment posed by separated flows through which lasers are projected could reduce the lasers' lethality to 1% of its otherwise diffraction-limited performance.[1]

The fast-evolving convecting turbulent structures that are present in turbulent flows and responsible for the aberrations usually exhibit high spatial and temporal bandwidths. Therefore, premier among the instruments' characteristics to acquire optical wavefronts is their ability to capture long time series of time-resolved, high-bandwidth, two-dimensional (2-D) wavefronts. To resolve the important aberrations, temporal bandwidths must exceed 50 kHz. This minimum frequency threshold is defined for two reasons. The first reason applies to acquiring data to characterize an aero-optical environment. One of the most bandwidth demanding environments is a turbulent boundary layer, which typically can have aberrations occurring at frequencies up to 20 kHz. Being able to acquire at more than twice that would achieve a minimum Nyquist criterion to be able to make measurements. Furthermore, if the wavefront sensor is contemplated for use as part of a conventional adaptive optic (AO) system, 50 kHz is really a lower bound. Rules of thumb for conventional AO systems are that the gains are typically on the order of 0.1 and restoration of high Strehl ratios requires approximately 10 corrections per disturbauce cycle; this means that a 50-kHz wavefront sensor can robustly correct only a 500-Hz aberration. Thus, bandwidths in excess of 50 kHz

really set a minimum threshold for use on aero-optical effects. Most commercially available 2-D wavefront sensors rely on a digital charge-coupled device (CCD) camera and, although it usually provides an excellent spatial resolution, sampling rates are typically limited to a few hundred frames per second. These rates are far lower then desired sampling frequencies to correctly resolve optical aberrations, which are on the order of tens of kilohertz. Furthermore, in a wind-tunnel testing environment, aberrations caused by aero-optical flows of interest must be separated from other wavefront aberrations that are necessarily superimposed on the wavefronts due to the testing environment, such as tunnel/floor vibrations, and temperature variations in the main tunnel flow and flow over insertion and extraction windows, to name a few.[12]

One way to get around a limitation on temporal sampling caused by a commercially available CCD camera is to replace it with an analog sensor. We have developed and successfully tested a high-speed analog Shack–Hartmann sensor, which utilizes an 8×8 array of analog position-sensing devices. A sampling rate of 78 kHz was shown, and it was limited only by the data acquisition system chosen. It provides continuous, long time series of the wavefronts' evolution, to which vibration handling procedures can be applied.

A test experiment using a slightly heated, low-speed planar jet was conducted to verify the validity and accuracy of a high-bandwidth wavefront sensor. A low-speed commercially available 2-D wavefront sensor was used to make benchmark measurements. Streamwise evolution of roll-up structures and its convective nature, as well as an amplitude of optical aberrations, were correctly captured in the wavefronts by using the high-speed wavefront sensor.

2. Heated-Jet Facility

2.1. Facility description

The heated-jet facility is shown schematically in Fig. 1a. It consists of a plenum chamber pressurized above atmospheric pressure by a squirrel-cage-type blower. After passing through filters and a slight contraction, air enters a rectangular duct with a series of heaters

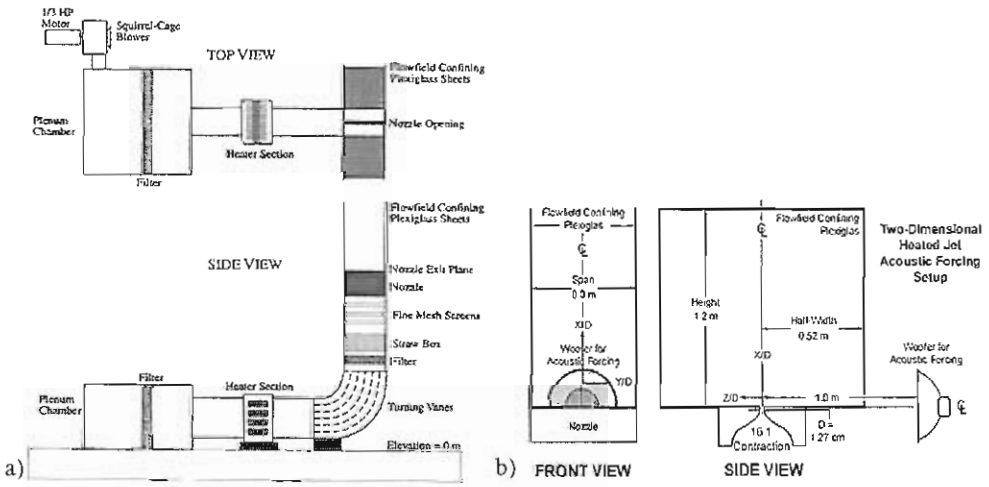

Fig. 1. (a) 2-D heated-jet facility[9]; (b) schematic of heated-jet exit plane.

located approximately 1 m from its entrance and 1 m from a 90-deg finned bend so that the heated air is now moving vertically in a rectangular duct with filters and flow straighteners, as shown in Fig. 1a. The flow then passes through a 16:1 2-D nozzle to an exit nozzle of width D 12.7 mm. The heated jet leaves the nozzle with a core velocity of 10 m/s. The detailed fluid mechanic measurements for this jet can be found in Ref. 9.

Figure 1b is a schematic of the exit plane of the nozzle and an associated system of coordinates. On the left is a view normal to the span of the jet (the optical beam path) showing the span dimension, 30 cm, and the end plates aligned in the flow direction to help reduce three-dimensional effects that would otherwise be present if the jet were uncontained. On the right is a view along the cross-stream direction of the jet showing a number of important details. First, the jet exit plane forms a solid floor that extends for 0.52 m in each direction from each edge of the nozzle. Second, the location and orientation of a speaker used to force the flow is shown; this speaker is located perpendicular to the exit plane, 1 m from the center line of the nozzle in the $+z$ direction.

2.2. Jet's response to acoustical forcing

The details of the jet's response to acoustic forcing can be found in Refs. 2 and 3. It is sufficient here to briefly describe the jet's characteristics used for the comparisons reported here. The acoustic forcing was provided by a 600-W Pyramid PWFX107 10-in. woofer located as shown in Fig. 1b. The speaker was driven by a Crown CE2000 power amplifier with an input provided by an Agilent Model 33120A function/arbitrary waveform generator. In the present case the jet was forced with a 240-Hz sine waveform.

The jet's response to the 240-Hz forcing was to regularize the jet's most unstable Kelvin–Helmholtz instability in the jet's two free shear layers. Depending on the amplitude of the acoustic signal, the first roll-up can be adjusted closer to or farther away from the nozzle exit plane. The forcing also regularizes the first pairing, resulting in the formation of 120-Hz subharmonic, larger-coherence-length flow structures; however, this regularization is slightly less robust than the first roll-up. To provide the best 120-Hz regularization, the amplitude of the acoustic signal caused the 240-Hz roll-up to occur somewhat closer to the exit plane than used and reported in earlier studies, which concentrated primarily on the 240-Hz structures.[10,13] In these earlier studies, the 2-D heated-jet facility was acoustically forced in a manner similar to the present experiment. A smoke visualization of the jet and the phase-locked-averaged temperature field collected for the forced jet is shown in Fig. 2. This figure shows the effect that the acoustic forcing had on the jet's optical path difference (OPD) pattern. Figure 3a is the heated jet's OPD pattern without acoustic forcing. One should note that the OPD peaks are quite random, and while there is a certain temporal frequency to this pattern, there is also a large standard deviation about this frequency. Figure 3b shows that acoustic forcing regularizes both the amplitude of the OPD and the temporal frequency of the pattern. It is this predictable, repeatable OPD pattern that was used to calibrate the wavefront measurement devices for this study.

3. High-Bandwidth Wavefront Sensor

3.1. Commercially available Wavefront Sciences wavefront sensor

Before discussing the high-bandwidth wavefront sensor, a typical commercially available wavefront sensor, such as the Wavefront Sciences CLAS-2D wavefront sensor, will be

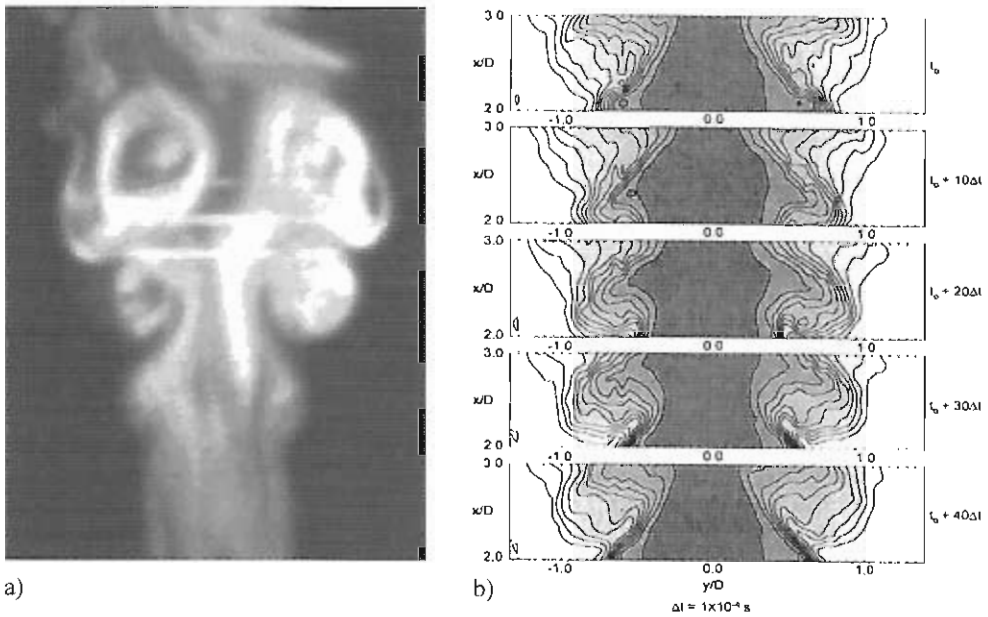

Fig. 2. Smoke visualization of the 2-D heated jet (a) and phase-averaged temperature profiles of the jet (b).[10]

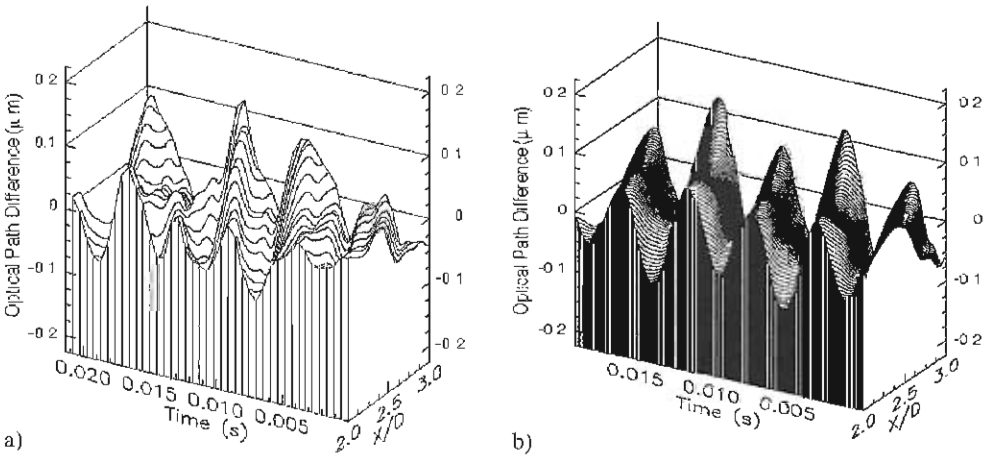

Fig. 3. Time series of experimentally measured OPDs from propagation through a two-dimensional heated jet (a) without acoustic forcing[13] and (b) with acoustic forcing.[11]

described. This wavefront sensor is a traditional Shack–Hartmann sensor,[5] and the principle of operation is shown in Fig. 4. The incoming wavefront is intercepted by a lenslet array, and an average wavefront slope over each lens subaperture is qualified by measuring dot displacements at the focal plane. These displacements $\boldsymbol{d}$ are related to a gradient of a wavefront as $\text{grad(WF)} = -\tan(-\boldsymbol{d}/f) \approx -\boldsymbol{d}/f$, where f is a focal distance of a lenselet array. Knowing slopes at finite points, the wavefront is reconstructed using either a direct or an iterative method, for instance the Southwell method.[16] The displacement sensor head

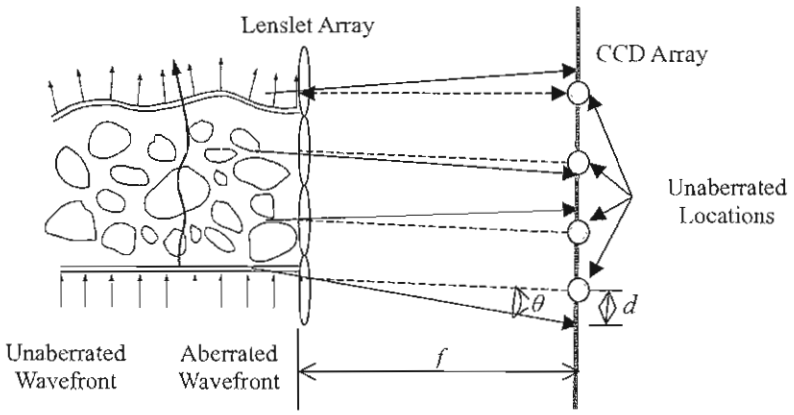

Fig. 4. Shack–Hartmann sensor: principle of operation.

itself is a CCD camera (without a lens) with, in the present case, a 33 × 44 lenslet array permanently aligned and mounted over the CCD array at the lenslet focal distance. The camera is framed by an off-the-shelf frame grabber, which in the present case can be single-frame externally triggered or can be run at a framing rate of 30 Hz. Clearly, the framing rate is insufficient to time resolve aero-optical flows of any practical importance; however, in the present case, with the heated jet acoustically forced as described in an earlier section, a pseudo-time-resolved time series of phase-locked-averaged wavefronts can be collected for the purpose of comparison with time-resolved, wavefront measuring instruments.

It is important to note that both piston and tilt must also be removed from the 2-D wavefronts, that non-time-resolved wavefronts contain no frequency information, and that vibration contamination can be removed only by assuming that the average tilt over the aperture is due solely to vibration.

3.2. High-bandwidth wavefront sensor

Commercially available wavefront sensors use a CCD array and postprocessing algorithms to determine beam centroid positions. CCD sensors typically satisfy and exceed the spatial requirements for a wavefront sensor to perform testing for aero-optics; however, no sensor can even approach the temporal bandwidth needed to properly study aero-optical effects as laid out in the preceding sections. Typical so-called high-speed wavefront sensors are bandwidth limited to approximately 1 kHz, a shortfall of almost two orders of magnitude from the bandwidth requirements detailed above.

To address the temporal bandwidth shortfall inherent in CCD-based sensors, Notre Dame developed a Shack–Hartmann sensor using an array of analog position-sensing devices (PSDs) to capture focal plane beam centroid displacements. Replacing the CCD array with an array of analog PSD devices that have response rates in excess of 200 ns allows for a significant increase in temporal sampling rates up to hundreds of kilohertz. This analog sensor comprises four individual, 4 × 4 arrays configured in a modular fashion to compose a contiguous 8 × 8 array. The performance of one such individual 4 × 4 array was reported in Ref. 7. Combined 4 × 4 units to obtain an overall 8 × 8 PSD-based sensor are shown in Fig. 5a. Each sensor obtains a centroid dot location by measuring currents on all four

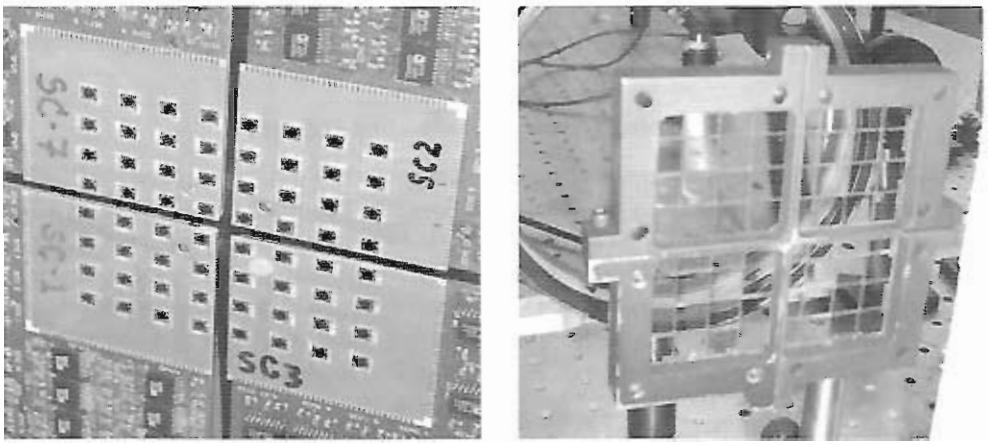

a) b)

Fig. 5. 8 × 8 high-bandwidth sensor array: (a) four boards with 64 PSDs; (b) 8 × 8 lenslet array.

sensor's edges. After a proper calibration, currents can be converted into instantaneous dots' positions with a sampling speed limited only by a given analog/digital (A/D) board.

A 8 × 8 lenslet array consisting of 64 square lenses with total size of 80 × 80 mm and 100% fill ratio is presented in Fig. 5b. A relatively big focal distance $f = 0.5$ m gives a better signal-to-noise ratio. For this 8 × 8 sensor a capture rate of 78,125 Hz has been demonstrated; as was mentioned before, this sampling rate is defined only by an A/D board in use.

4. Heated-Jet Wavefront Results

4.1. Baseline flow

The heated-jet facility at Notre Dame, shown in Fig. 1, was used as a benchmark flow to characterize different wavefront sensors in Ref. 4, and the interested reader is referred to this paper for an extensive discussion about the flow quality and a complete description of the flow structure. Here we will highlight only the essential features of the flow. The flow is acoustically forced at 240 Hz with a speaker to expedite and stabilize the development of the vortical structure, as seen in Fig. 2a. The first roll-up occurs at $x/D = 1$, with a subsequent structure pairing occurring at approximately $x/D = 2.0...2.5$, where $D = 12.7$ mm is the jet width.

To acquire wavefronts with the CLAS-2D wavefront sensor in the streamwise direction for a range of $x/D = 0.5...2.5$, a helium–neon (He–Ne) collimated laser beam of 25-mm diameter was propagated through the jet parallel to the jet's exit plane (i.e., along the z direction) and directed onto the optical bench using beam-steering mirrors. In a separate experiment, the high-bandwidth sensor described here used a continuous-wave neodinium Yag (YaG:Nd) laser operating in the 532-nm wavelength capable of 2 W of power. The laser beam was expanded to a 25-mm-diameter collimated beam and, after passing through the same location in the jet as for the He–Ne laser, was expanded to a 100-mm beam and directed to the high-bandwidth sensor using steering mirrors. Only a central square portion

of the wavefront the size of the lenslet array was sampled, which corresponds to a jet's streamwise locations of $x/D = 0.7...2.3$.

4.2. Comparison of wavefront sensors

The CLAS-2D wavefront sensor was used to capture series of phase-locked wavefronts using 240-Hz forcing frequency as a locking frequency. The results in Fig. 6 show two-dimensional wavefronts, phase-locked to the 40-Hz forcing frequency, collected with the Wavefront Sciences sensor. When the jet is acoustically locked, as in these experiments, the presumption is that the jet becomes two-dimensional, that is, the flow structure in the x direction is repeated at all span y locations. The 2-D wavefronts in Fig. 6 indicate that this presumption, although not perfect, is closely approximated by the flow. Further, the

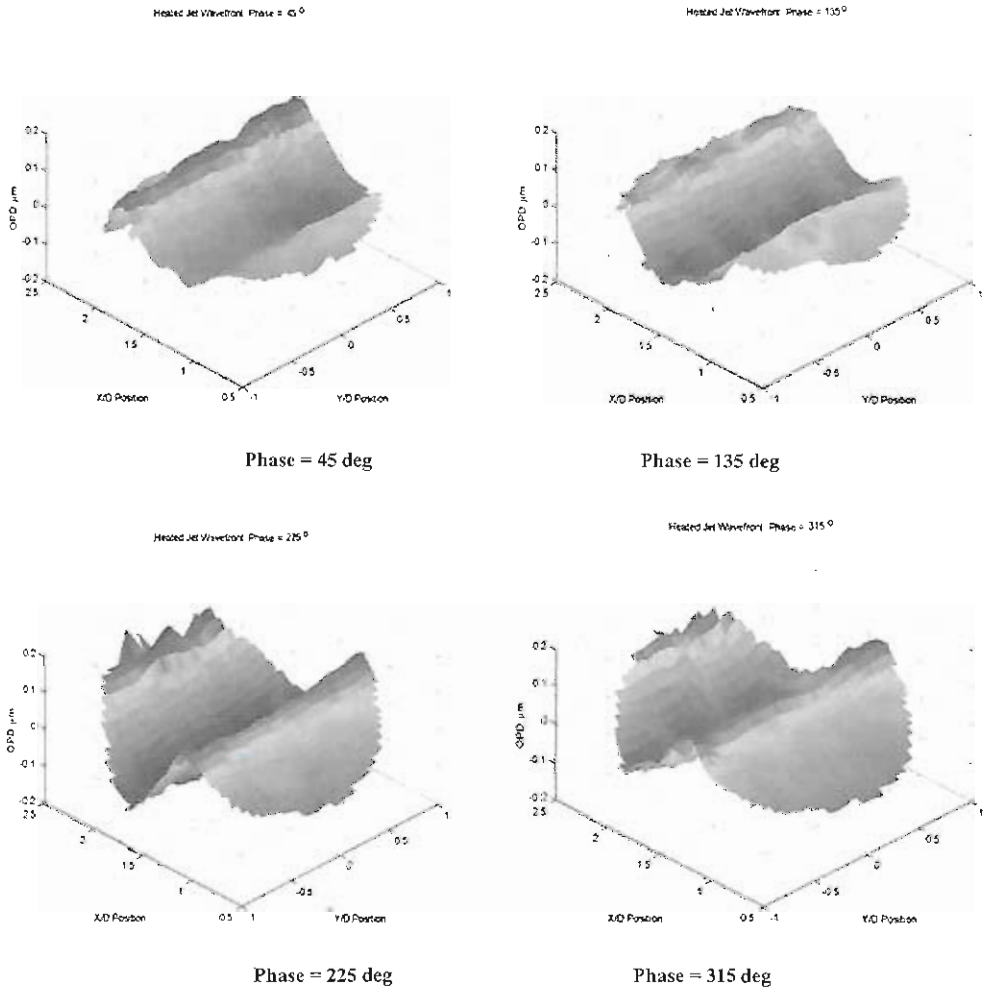

Fig. 6. Typical instantaneous wavefronts obtained with the Wavefront Sciences CLAS-2D wavefront sensor at various phase angles ($-1.0 < Y/D < 1.0$; $0.5 < X/D < 2.5$; OPD scale in microns).

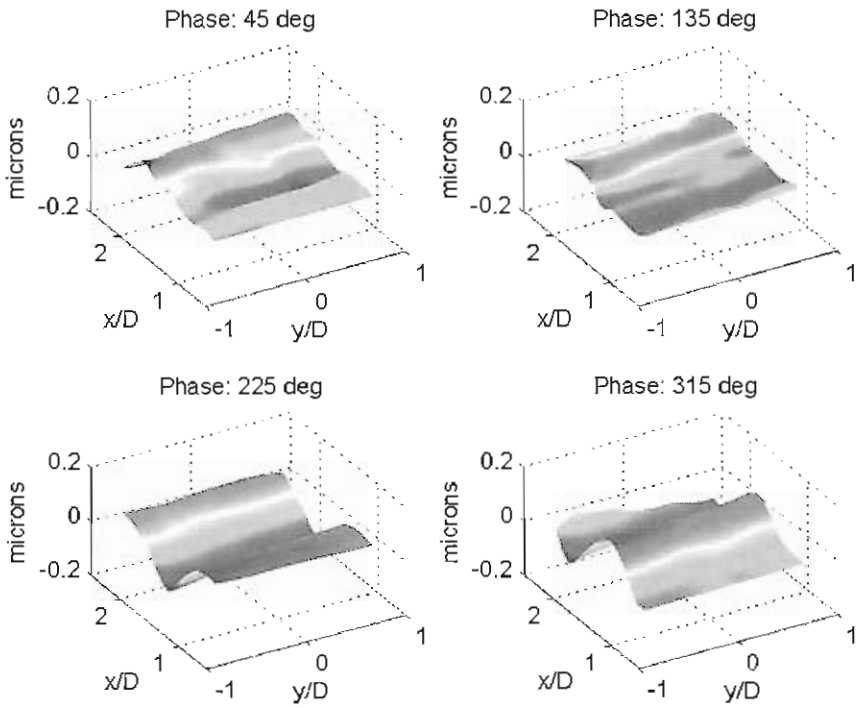

Fig. 7. Phase-averaged wavefronts obtained with the 8×8 high-bandwidth wavefront sensor.

convective nature of the aberration through the aperture is clearly apparent in the realizations. Roll-up of the first aberrating structure can he seen to be clearly developed after $x/D = 1$, with the wavefront amplitude being around 0.1 μ. A sampling rate of 78 kHz was used to acquire wavefronts using the high-bandwidth wavefront sensor. Data were phase-locked to the 240-Hz forcing frequency and averaged over 200 ensembles to get phase-averaged wavefronts. Results for selected phases are presented in Fig. 7. A comparison with highly spatially resolved phase-locked wavefronts using the CLAS-2D wavefront sensor (Fig. 6) revealed that although the high-bandwidth wavefront sensor has only a modest spatial resolution of 8×8 apertures, it captures all essential features of the flow-indnced aberrations, including the development of the roll-up structure hy $x/D = 1$, its spanwise-uniform nature, and even evidence of pairing events around $x/D = 2$.

A comparison of both wavefront-sensing techniques over an aperture from $x/D = 0.5$ to $X/D = 2.5$ is given in Fig. 8. Both the CLAS-2D and the high-bandwidth wavefront sensors data were averaged in the spanwise direction to get one-dimensional slices of wavefronts along the streamwise direction. Figure 8 not only shows that both wavefront sensors' peak-to-peak amplitude measurements are of the same order but that many essential flow features are captured by both sensors. The CLAS-2D wavefront sensor gives a good spatial resolution of the underlying flow structure, but it is clear that eight subapertures in the streamwise direction used in the high-bandwidth wavefront sensor are sufficient to resolve the main roll-up structure and correctly measure its position and amplitude. It is important to note that the optical signal has a modest peak-to-peak amplitude of no more than 0.2 μ, yet the high-bandwidth wavefront sensor was able to correctly resolve optical wavefronts.

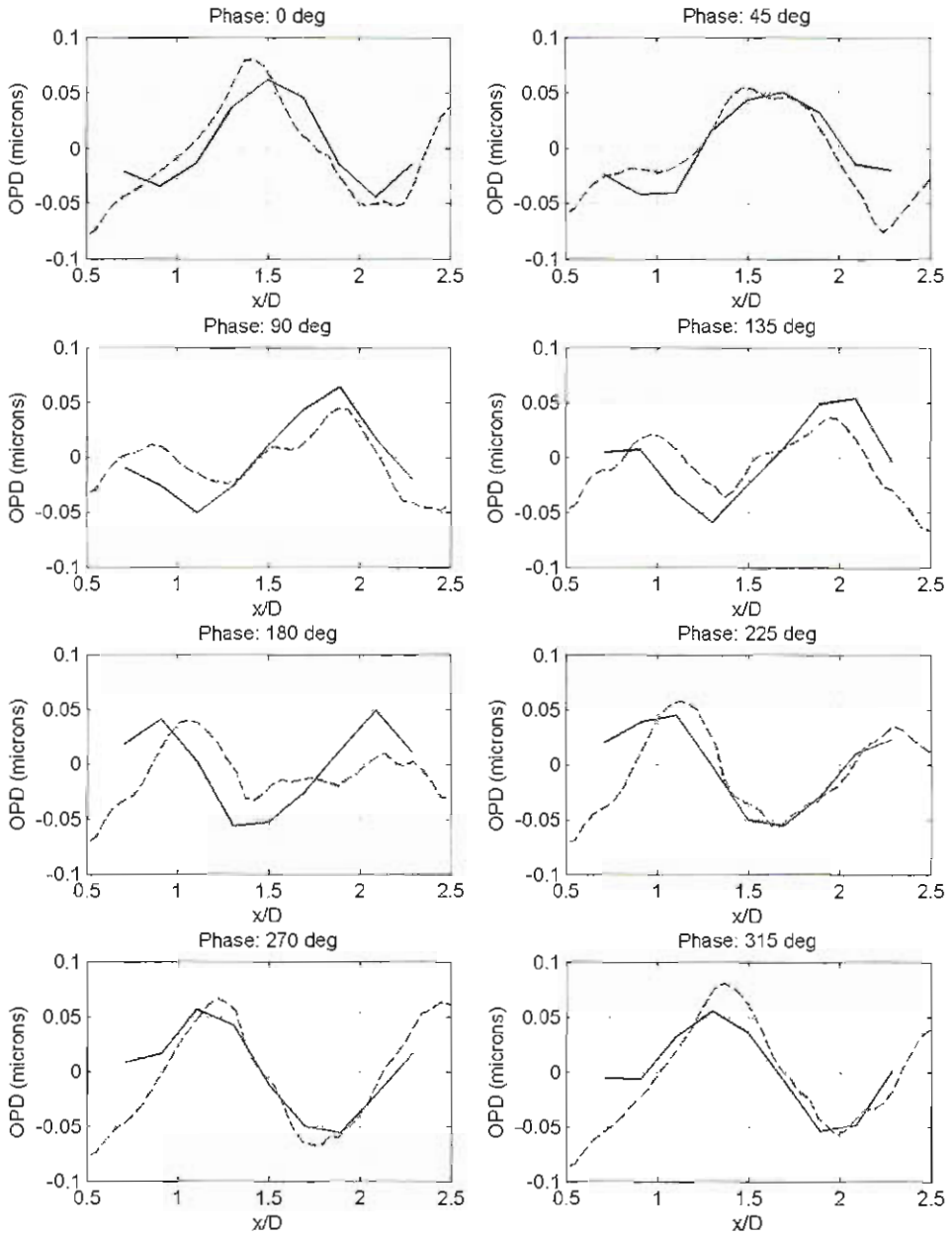

Fig. 8. Phase-averaged wavefronts obtained with the high-bandwidth wavefront sensor (——) and commercial WF sensor (– – –) at various phase angles.

5. 8 × 8 Sensor as Multibeam Malley Probe

The high-bandwidth wavefront sensor provides highly sampled time series of deflection angles averaged over subapertures for all subapertures, so it can be viewed as a multibeam Malley probe sensor. As was shown in Ref. 15, applying a spectral cross-correlation method

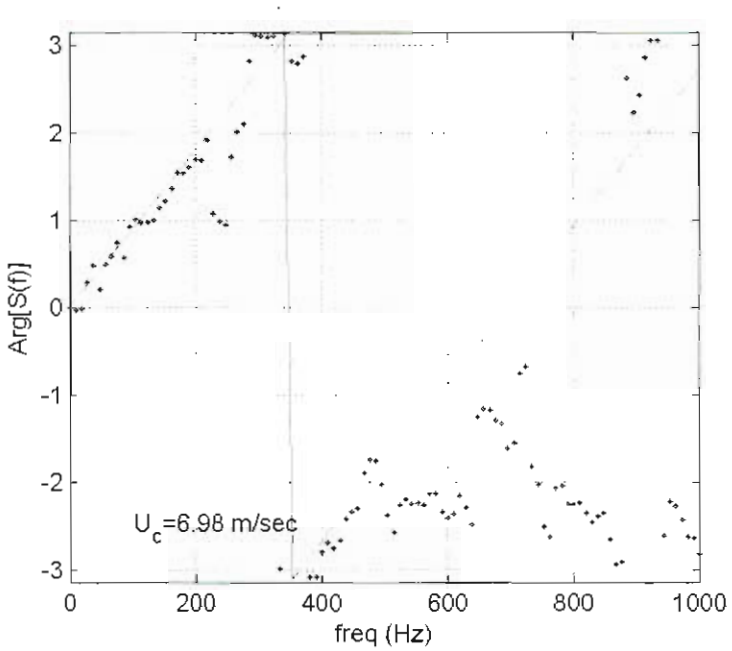

Fig. 9. Phase plot of the deflection angle cross correlation between two sensors on the 8×8 sensor. The lines are the linear fits.

between two beams spaced in the streamwise direction provides unique information about frequencies contaminated by vibrations, which permits removal or handling of vibrations unambiguously. In addition, by measuring the slope of an argument (a phase) of the cross-correlation function, one can obtain an average convective speed of optical aberrations at a beam's location.[8] For pure convective structure the phase plot is a linear function of frequency and the slope is related to the local convective speed. The phase plot of the spectral cross correlation between two sensors in the middle of the sensor board is shown in Fig. 9. The phase is indeed linear for a range of frequencies between 0 and 500 Hz. The solid line is a linear fit to data at this range, and the resulting convective speed was found to be around 7 m/s.

6. Real-Time Logging

Most wavefront reconstruction techniques are performed as a part of a postprocess analysis, mostly because data are sampled fast in digital form but require a significant postprocessing time using a computer with proper software. Mathematically, wavefront reconstruction from deflection angles is a linear matrix multiplication. These manipulations can be done on-line using an analog circuitry, which produces wavefronts as an output signal. The current 8×8 sensor has a capability of logging out wavefronts at speeds up to 32 kHz. The output can directly control a deformable mirror, which is an essential component of any live wavefront correction scheme. Thus, the 8×8 sensor can be used to measure instantaneous wavefronts and apply open- or closed-loop control strategies to reduce optical aberrations on the outgoing beam at speeds up to 32 kHz.

7. Conclusions

A high-bandwidth wavefront analog sensor with 8 × 8 spatial resolution was successfully developed and tested against a commercially available high-spatial-resolution wavefront sensor using a slightly heated low-speed jet as a benchmark flow. The high-bandwidth sensor was able to measure instantaneous wavefronts at sampling speeds up to 78 kHz as a postprocess analysis, when raw data were just sampled at this speed, but data were converted to wavefronts off-line. Also, the sensor is able to provide real-time wavefront calculations at speeds up to 32 kHz, and it can directly control a deformable mirror used in most adaptive optics control strategies.

Performing a spectral cross correlation between sensors provides an objective means of identifying vibration-related frequencies and their subsequent removal from wavefronts. In addition, it provides local convective speeds of optically active structures. A modular design permits the reconfigurion of the 8 × 8 sensor to a 4 × 8 or 4 × 16 sensor, if needed.

References

[1]Cicchiello, J., and E. Jumper, Appl. Opt. 36(25), 6441 (1997).

[2]Duffin, D., "Feed-Forward Adaptive Optic Correction of Aero-Optical Aherrations Caused by a Two-Dimensional Heated Jet," AIAA Paper 2005-4776, 36th AIAA Plasmadynamics and Lasers Conference, Toronto, Ontario, Canada, June 6–9, 2005.

[3]Duffin, D., S. Gordeyev, and E. Jumper, "Comparison of Wavefront Measurement Techniques on a Two-Dimensional Heated Jet," AIAA Paper 2004-2406, June 2004.

[4]Duffin, D.A., S. Gordeyev, and E.J. Jumper, "Visualizing Index-of-Refraction Variations in Optically Active Flow Fields," Paper 075, 11th International Symposium of Flow Visualization Conference, Notre Dame, IN, 2004.

[5]Geary, J.M., "Introduction to Wavefront Sensors," *Tutorial Texts in Optical Engineering*, Vol. TT18, SPIE Optical Engineering Press, Bellingham, WA (1995).

[6]Gilbert, K.J., and L.J. Otten (eds.), *Aero-Optical Phenomena*, Progress in Astronautics and Aeronautics, Vol. 80, AIAA, New York (1982).

[7]Gordeyev, S., D. Duffin, and E. Jumper, "Aero-Optical Measurements Using Malley Probe and High-Bandwidth 2-D Wavefront Sensors," V0020, International Conference on Advanced Optical Diagnostics in Fluids, Solids and Combustion, Tokyo, Japan, December 4–6, 2004.

[8]Gordeyev, S., E.J. Jumper, T. Ng, and A. Cain, "Aero-Optical Characteristics of Compressible, Sub-Sonic Turbulent Boundary Layers," AIAA Paper 2003-3606, June 2003.

[9]Hugo, R.J., "Quantifying the Spatio-Temporal Effects of Optically-Active Turbulent Flowfields on a Coherent Optical Wave," Ph.D. Dissertation, Department of Aerospace and Mechanical Engineering, University of Notre Dame, Notre Dame, IN, 1995.

[10]Hugo, R.J., and E.J. Jumper, "Implications of the Homogeneous Turbulence Assumption on the Aero-Optic Linking Equation," in *Optical Techniques in Fluid, Thermal, and Combustion Flow*, Vol. 2546, edited by S.S. Cha and J.D Trolliuger, SPIE—International Society of Optical Engineering, Bellingham, WA, pp. 189–200 (1995).

[11]Hugo, R.J., and E.J. Jumper, "Constant Current Anemometry and Its Impact ou Aero-Optical Measurements," AIAA Paper 95-1986, June 1995.

[12]Hugo, R.J., and E.J. Jumper, AIAA J. 33(11), 2151 (1995).

[13]Hugo, R.J., and E.J. Jumper, Appl. Opt. 35(22), 4436 (1996).

[14]Jumper, E.J., and E.J. Fitzgerald, Prog. Aerospace Sci. 37, 299 (2001).

[15]Malley, M., G.W. Sutton, and N. Kincheloe, Appl. Opt. 31, 4440 (1992).

[16]Southwell, W.H., J. Opt. Soc. Am. 70(8), 998 (1980).